Electronic Supplementary Information

MnO_x-decorated MOF-derived nickel-cobalt bimetallic phosphides nanosheet arrays for overall water splitting

*Zheng Zhang,[a] Lei Han,[a] and Kai Tao[a]**

[a] School of Materials Science & Chemical Engineering, Ningbo University, Ningbo, Zhejiang 315211, P. R. China.

E-mail: taokai@nbu.edu.cn

Fabrication of control NiCo-LDH nanosheets on NF (NiCo-LDH-con/NF):

First, 0.291g $Co(NO_3)_2 \cdot 6H_2O$, 0.291g $Ni(NO_3)_2 \cdot 6H_2O$, 0.3g urea and 0.092g NH_4F were dissolved in 30 mL DI water to form the solution. Then, the solution was transferred to a 50 mL autoclave. Subsequently NF (2*3 cm^2) was placed into the solution as a conductive substrate and heated at 120 ^oC for 6 h. After cooling to room temperature, the NiCo-LDH-con/NF was obtained.

Characterization

The crystalline structure of the sample was characterized with X-ray diffractometer (Bruker AXS D8 Advance). The compositions and microstructures of the samples were analyzed by field emission scanning electron microscope (FESEM, Hitachi S-4800) and transmission electron microscope (TEM, FEI Talos F200x) equipped with an energy dispersive X-ray spectrometer (EDS). X-ray photoelectron spectroscopy (XPS) measurements were performed using a Thermo Scientific K-Alpha spectrometer.

Electrochemical measurements

All electrochemical measurements were carried out by using a CHI660E electrochemical workstation in 1.0 M KOH with a three-electrode system, where the

as-prepared samples (geometric area: 1.0 cm^{-2}), Pt mesh (1 cm×1 cm) and an Hg/HgO electrode were used as working, counter and reference electrode, respectively. All measured potentials were converted to potentials *vs* reversible hydrogen electrode (RHE): $E_{RHE}= E_{Hg/HgO} + 0.0592\times pH + 0.098$. Linear sweep voltammetry (LSV) was carried out at a scan rate of 2 mV s^{-1}, after the sample was activated by 150 cyclic voltammetry (CV) cycles (with a scan rate of 50 mV s^{-1}). All polarization curves were iR-corrected according to: $E_{corr}=E_m-iR_s$, where E_{corr} was iR-corrected potential, E_m was experimentally measured potential, and R_s was the equivalent series resistance obtained from the electrochemical impedance spectroscopy (EIS) measurement. The Tafel plots were were determined from LSV at 2 mV s^{-1} with 100% iR corrected and the slopes were calculated based on the equation: $\eta = b \log j + a$ where η, b and j are the overpotential, Tafel slope and current density, respectively. The EIS measurements for HER and OER are performed at frequencies ranging from 100 kHz to 0.1 Hz with potentials of -0.2 and 1.53 V, respectively. Double-layer capacitances were calculated from CV curves with various scan rates ranging from 20 to 100 mV s^{-1}. The stability of the electrode was evaluated by chronopotentiometry at different current densities. Bubbling method which recording data of the rising volume V (mL) of the soap bubble and the total number of charges transferred under constant current (250 mA cm^{-2}) was measured to calculate the Faraday efficiency (FE). ($FE=4*F*V/(1000*V_m*It$). Where F was the Faraday constant (96485 C mol^{-1}), V is the volume change of oxygen or H_2 production (mL) and V_m was the molar volume (molar under normal temperature and pressure, 24.5 L mol^{-1}). In a closed h-shaped electrolytic cell, H_2/O_2 gas production was measured via the drainage method. During 25 min of continuous electrolysis, the amount of water emitted by the anode and cathode was recorded every 5 min, and the volume of H_2/O_2 was subsequently recorded and compared with theoretical values as derived from the charge-time curve.

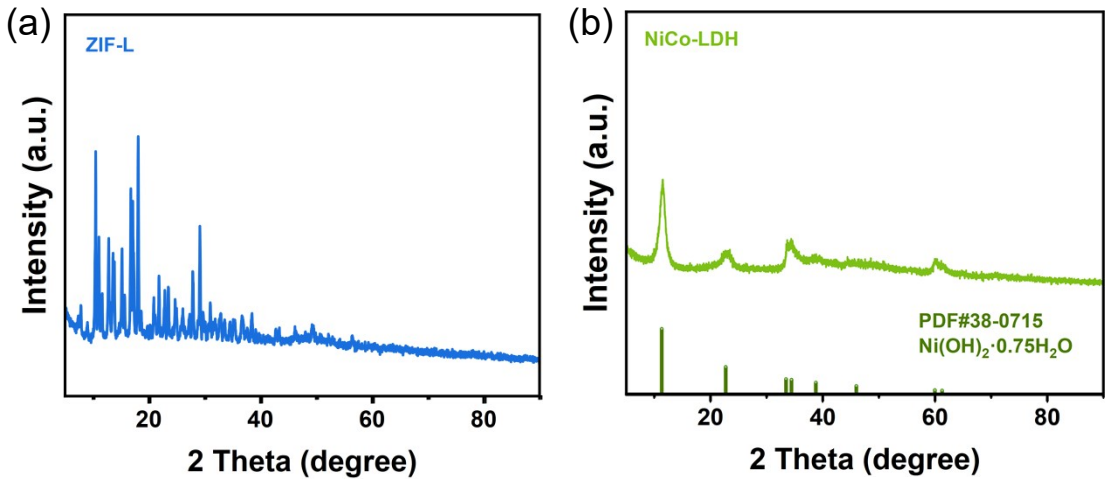

Figure S1. XRD patterns of (a) ZIF-L and (b) NiCo-LDH nanosheets.

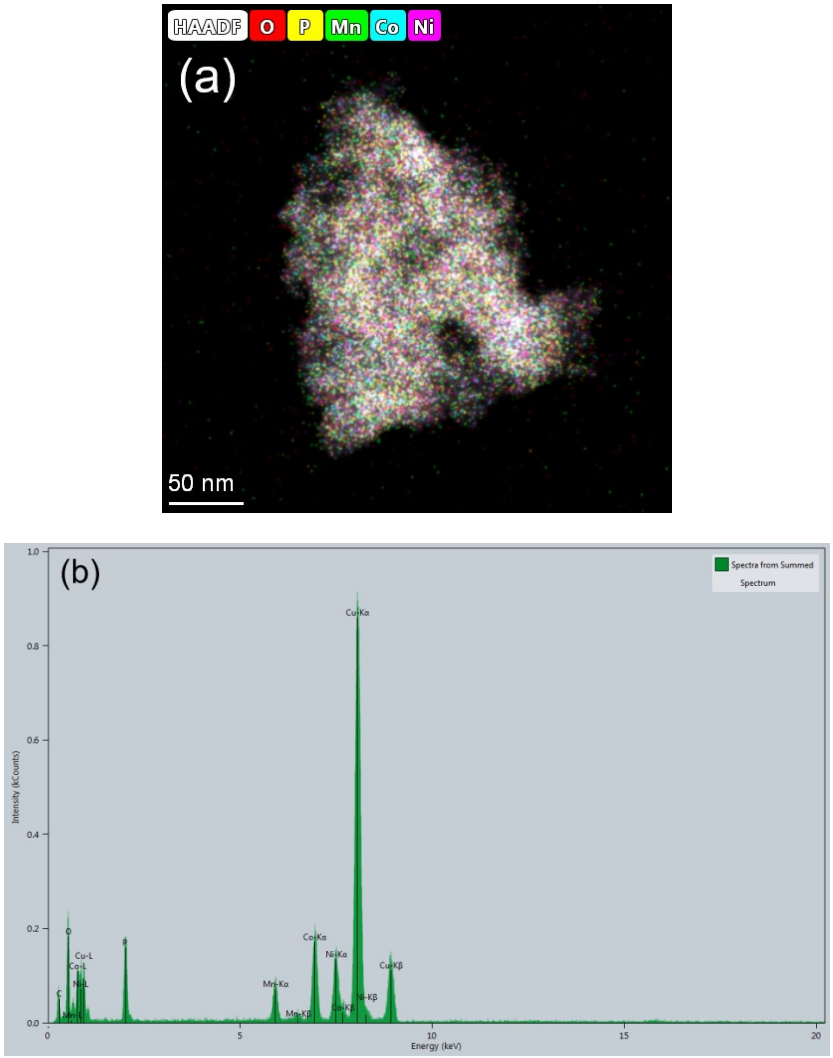

Figure S2. (a) HAADF image and (b) EDS pattern of MnO_x/NiCoP/NF.

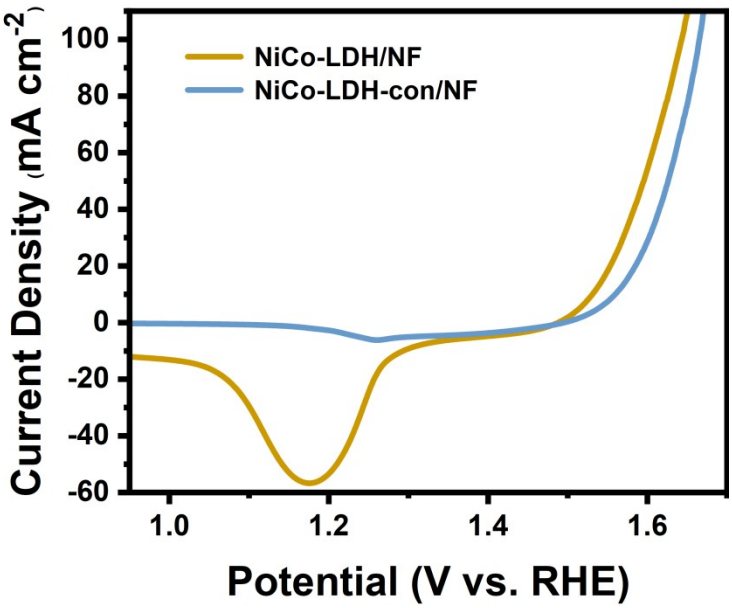

Figure S3. Comparison of the OER catalytic performance of MOFs-derived NiCo-LDH/NF and NiCo-LDH-con/NF prepared by a conventional hydrothermal method.

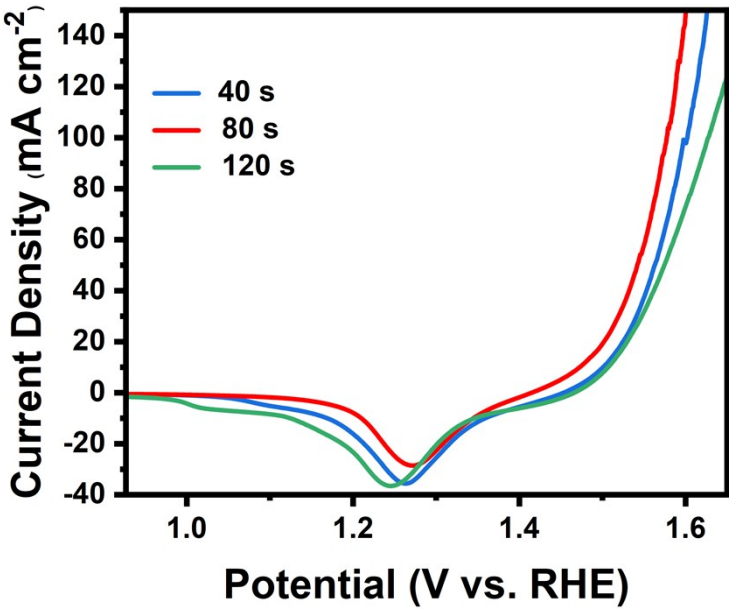

Figure S4. OER LSV curves of MnO_x/NiCoP/NF with different electrodeposition times.

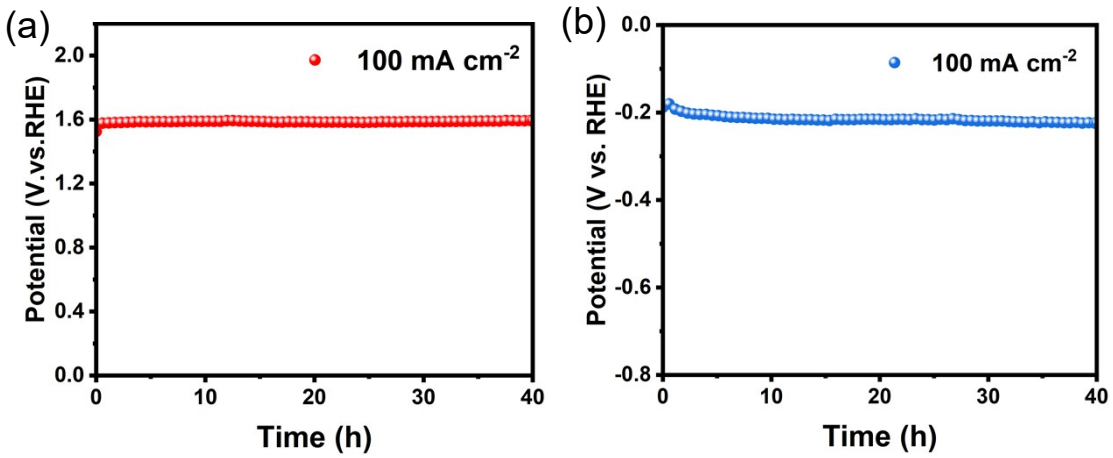

Figure S5. Durability test of (a) OER and (b) HER at 100 mA cm^{-2}.

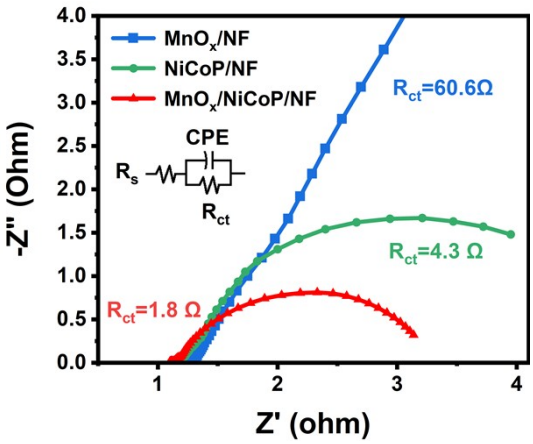

Figure S6. Nyquist plots for HER

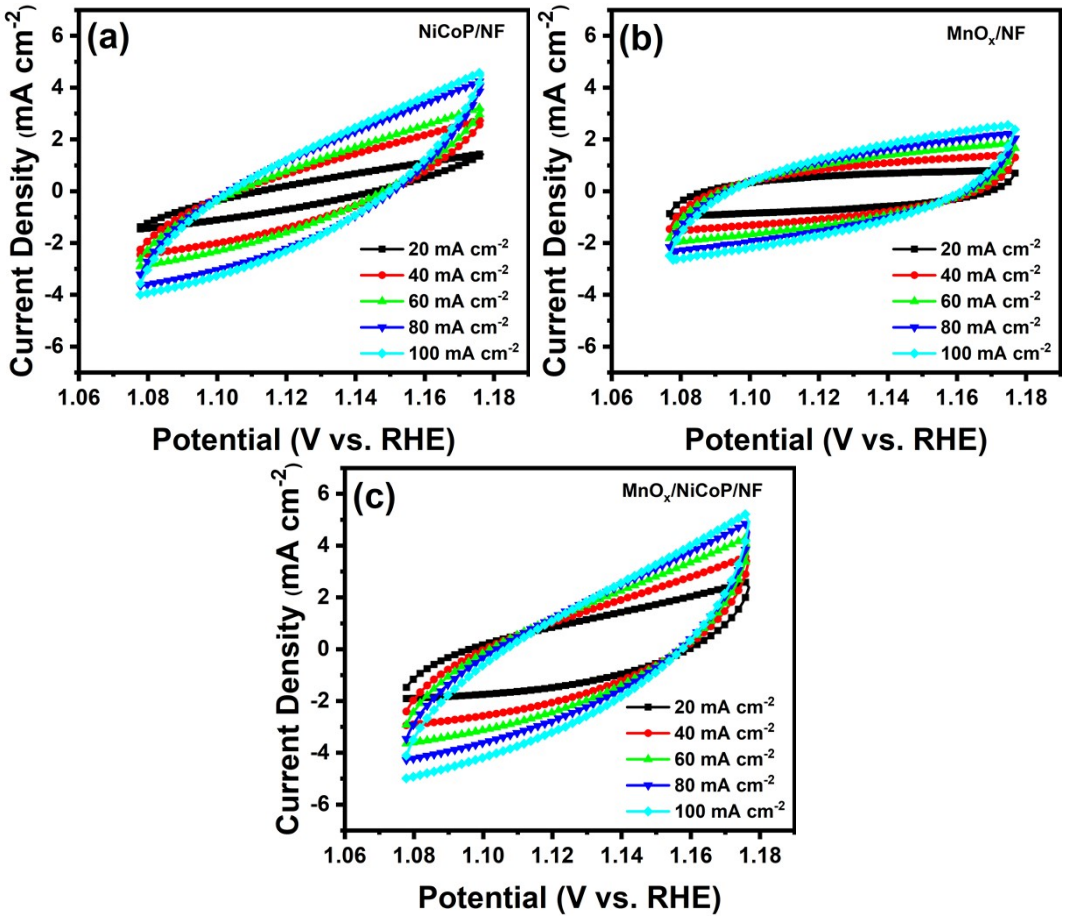

Figure S7. CV curves in the region of 1.0768V-1.1768V for (a) NiCoP/NF, (b) MnO_x/NF and (c) MnO_x/NiCoP/NF at various scan rates for OER.

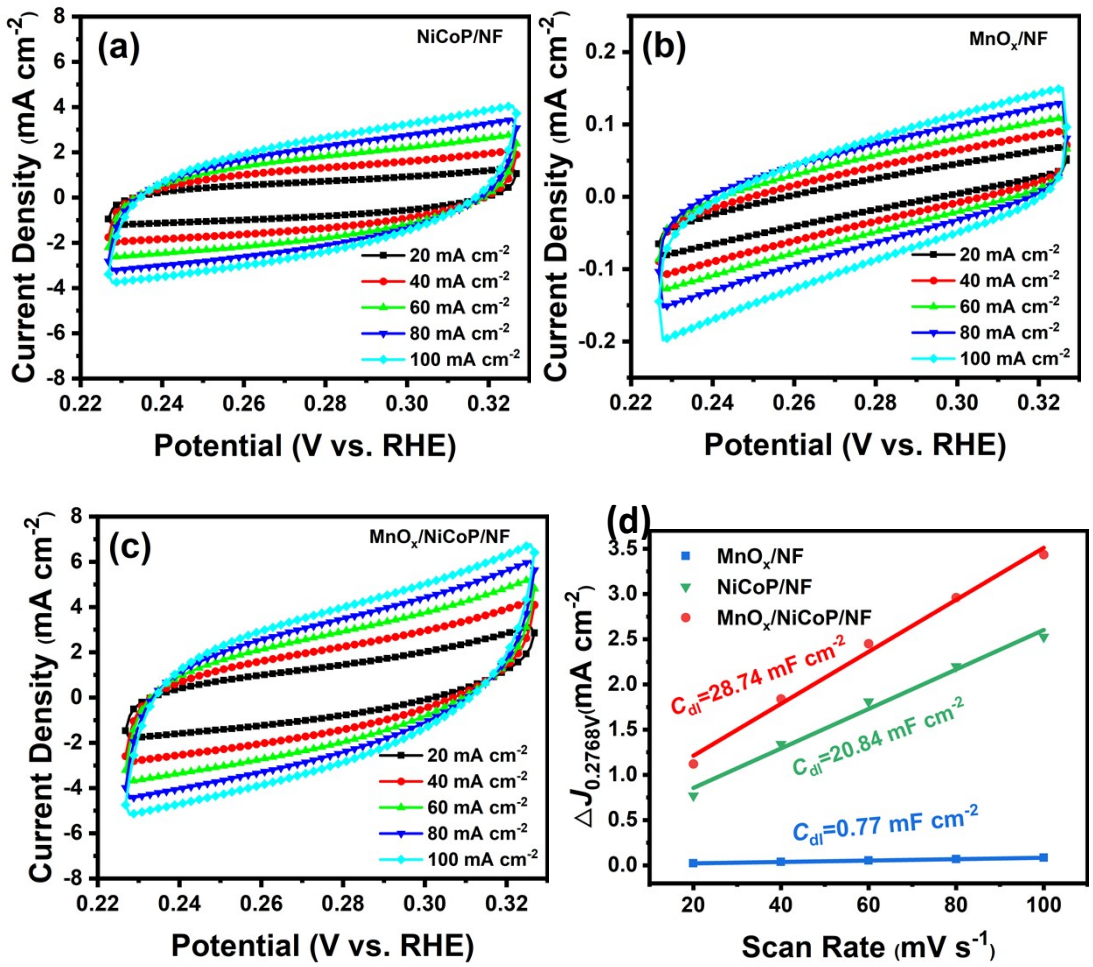

Figure S8. CV curves in the region of 0.2268V-0.3268V for (a) NiCoP/NF, (b) MnO_x/NF and (c) MnO_x/NiCoP/NF at various scan rates. (d) ΔJ at 0.2768 V as a function of scan rate for HER.

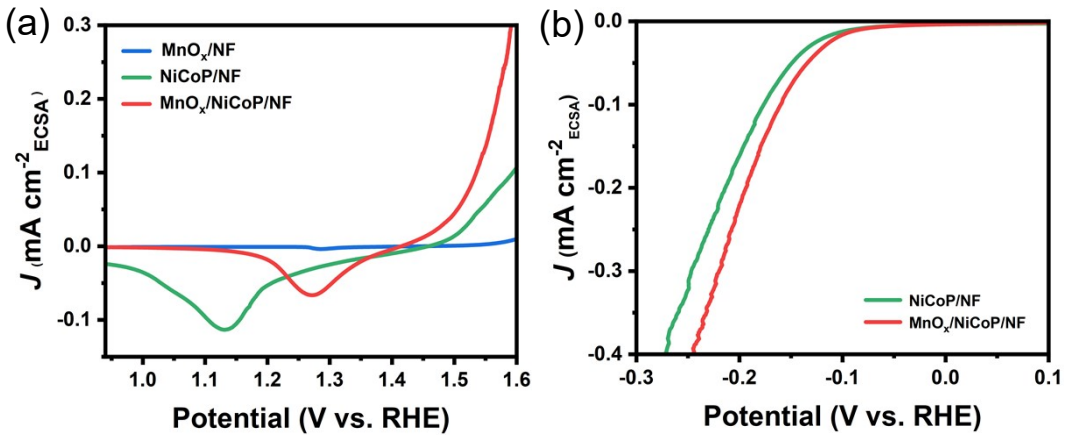

Figure S9. (a) OER LSV curves standardized by ECSA. and (b) HER LSV curves standardized by ECSA.

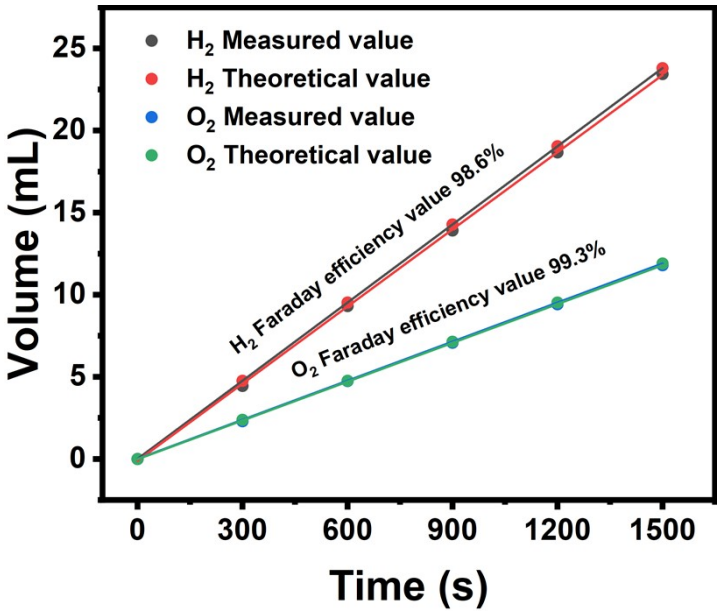

Figure. S10. Hydrogen efficiency and oxygen efficiency of MnO_x/NiCoP/NF|| MnO_x/NiCoP/NF under current density of 250 mA cm^{-2} in 1 M KOH.

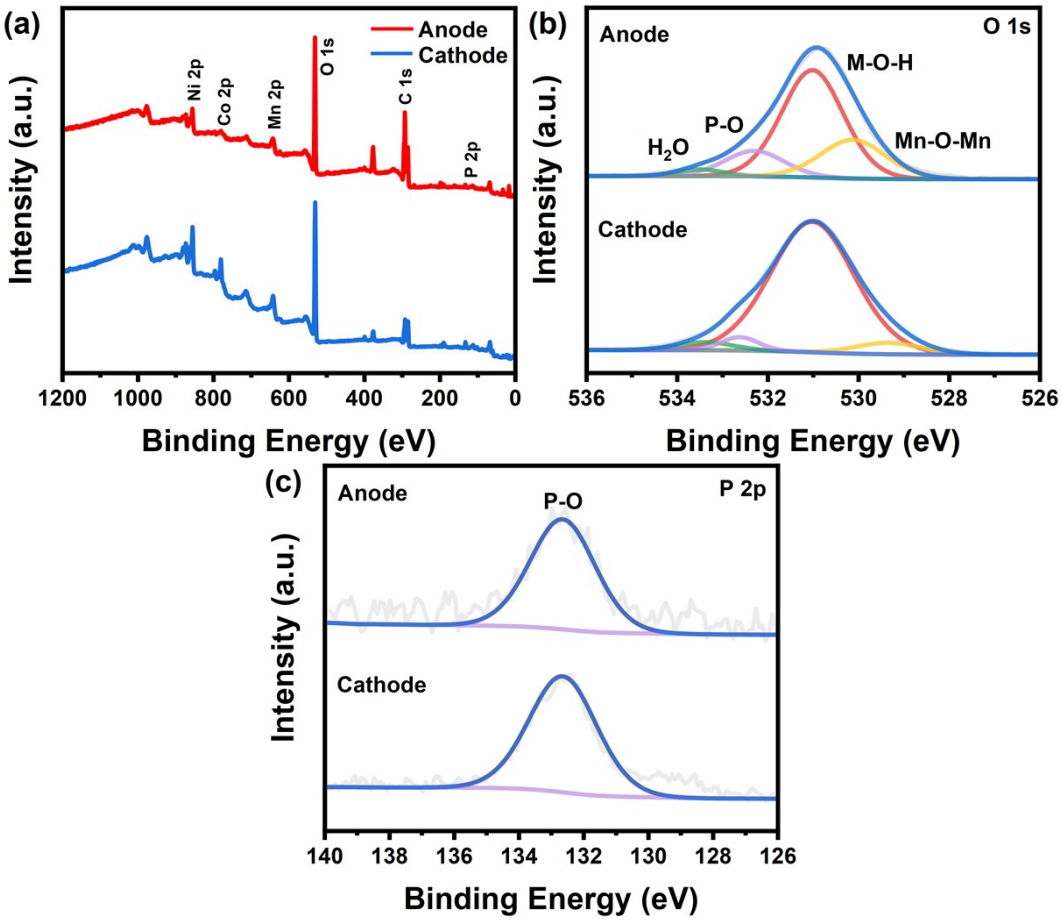

Figure. S11. (a) The survey XPS spectra, and corresponding high-resolution XPS spectra of (b) O 1s and (c) P 2p of MnO_x/NiCoP/NF as the cathode and anode after the chronopotentiometry measurement for overall water splitting.

Table S1. Element content and composition

Element	Atomic Fraction (%)	Mass Fraction (%)
O K	33.11	13.46
P K	17.83	14.03
Mn K	8.53	11.91
Co K	21.81	32.67
Ni K	18.72	27.92

TableS2.Comparison of the OER activity of MnO_x/NiCoP/NF with other non-noble metal electrocatalysts in alkaline solution.

Electrocatalyst	**j ($mA \cdot cm^{-2}$)**	**η(mV)**	**Electrolyte**	**Ref.**
MnO_x/NiCoP/NF	10	240	1M KOH	This work
$NiCo_{2-x}FeO_4$	10	274	1M KOH	1
NiCoP/NF	10	280	1M KOH	2
NiFeP/NF	10	264	1M KOH	3
NiCoP/CC	10	242	1M KOH	4
WCoFe/NF	10	250	1M KOH	5

TableS3.Comparison of the HER activity of MnO_x/NiCoP/NF with other non-noble metal electrocatalysts in alkaline solution.

Electrocatalyst	**j ($mA \cdot cm^{-2}$)**	**η(mV)**	**Electrolyte**	**Ref.**
MnO_x/NiCoP/NF	10	93	1M KOH	This work
Ni_2P/Co	10	149	1M KOH	6
CoP/NCNHP	10	115	1M KOH	7
CoP/Ni_2P	10	143	1M KOH	8
CoP/NPC/TF	10	118	1M KOH	9
N-C@CoP/Ni_2P	10	176	1M KOH	10

TableS4.Comparison of the overall water splitting activity of MnO_x/NiCoP/NF with other non-noble metal electrocatalysts in alkaline solution.

Electrocatalyst	**j ($mA \cdot cm^{-2}$)**	**η(V)**	**Electrolyte**	**Ref.**
MnO_x/NiCoP/NF	10	1.59	1M KOH	This work
Co_2P_{-x}/Ni_2P_{-y}@ NF	10	1.63	1M KOH	11
Co-P	10	1.64	1M KOH	12
$MnCo_2O_4$@Ni_2P/NF	10	1.63	1M KOH	13
NiCoFeP/C	10	1.60	1M KOH	14
$NiCo_2S_4$ NW/NF	10	1.63	1M KOH	15

References

1. Huang, Y.; Zhang, S. L.; Lu, X. F.; Wu, Z. P.; Luan, D.; Lou, X. W. D., Trimetallic Spinel NiCo(2-x) Fe(x) O(4) Nanoboxes for Highly Efficient Electrocatalytic Oxygen Evolution. *Angew Chem Int Ed Engl*, **2021,** *60*, 11841-11846.

2. Liang, H.; Gandi, A. N.; Anjum, D. H.; Wang, X.; Schwingenschlogl, U.; Alshareef, H. N., Plasma-Assisted Synthesis of NiCoP for Efficient Overall Water Splitting. *Nano Lett*, **2016,** *16*, 7718-7725.

3. Huang, H.; Yu, C.; Zhao, C.; Han, X.; Yang, J.; Liu, Z.; Li, S.; Zhang, M.; Qiu, J., Iron-tuned super nickel phosphide microstructures with high activity for electrochemical overall water splitting. *Nano Energy*, **2017,** *34*, 472-480.

4. Du, C.; Yang, L.; Yang, F.; Cheng, G.; Luo, W., Nest-like NiCoP for Highly Efficient Overall Water Splitting. *ACS Catalysis*, **2017,** *7*, 4131-4137.

5. Pi, Y.; Shao, Q.; Wang, P.; Lv, F.; Guo, S.; Guo, J.; Huang, X., Trimetallic Oxyhydroxide Coralloids for Efficient Oxygen Evolution Electrocatalysis. *Angew Chem Int Ed Engl*, **2017,** *56*, 4502-4506.

6. Li, S.; Zhang, Y.; Yuan, Y.; Chang, F.; Zhu, K.; Li, G.; Bai, Z.; Yang, L., Design and synthesis of dispersed Ni2P/Co nano heterojunction as bifunctional electrocatalysis for boosting overall water splitting. *International Journal of Hydrogen Energy*, **2023,** *48*, 3355-3363.

7. Pan, Y.; Sun, K.; Liu, S.; Cao, X.; Wu, K.; Cheong, W. C.; Chen, Z.; Wang, Y.; Li, Y.; Liu, Y.; Wang, D.; Peng, Q.; Chen, C.; Li, Y., Core-Shell ZIF-8@ZIF-67-Derived CoP Nanoparticle-Embedded N-Doped Carbon Nanotube Hollow Polyhedron for Efficient Overall Water Splitting. *J Am Chem Soc*, **2018,** *140*, 2610-2618.

8. Lv, X.; Tian, W.; Liu, Y.; Yuan, Z.-Y., Well-defined CoP/Ni2P nanohybrids encapsulated in a nitrogen-doped carbon matrix as advanced multifunctional electrocatalysts for efficient overall water splitting and zinc–air batteries. *Materials Chemistry Frontiers*, **2019,** *3*, 2428-2436.

9. Huang, X.; Xu, X.; Li, C.; Wu, D.; Cheng, D.; Cao, D., Vertical CoP Nanoarray Wrapped by N,P‐Doped Carbon for Hydrogen Evolution Reaction in Both Acidic and Alkaline Conditions. *Advanced Energy Materials*, **2019,** *9*, 1803970.

10. Feng, T.; Wang, F.; Xu, Y.; Chang, M.; Jin, X.; Yulin, z.; Piao, J.; Lei, J., CoP/Ni2P heteronanoparticles integrated with atomic Co/Ni dual sites for enhanced electrocatalytic performance toward hydrogen evolution. *International Journal of Hydrogen Energy*, **2021,** *46*, 8431-8443.

11. Zhao, H.; Liang, J.; Zhao, Y., Construction of hierarchical Co2P/Ni2P heterostructures on Ni foam as efficient bifunctional electrocatalyst for overall water splitting. *Journal of Alloys and Compounds*, **2022,** *907*, 164479.

12. Jiang, N.; You, B.; Sheng, M.; Sun, Y., Electrodeposited cobalt-phosphorous-derived films as competent bifunctional catalysts for overall water splitting. *Angew Chem Int Ed Engl*, **2015,** *54*, 6349-6352.

13. Ge, J.; Zhang, W.; Tu, J.; Xia, T.; Chen, S.; Xie, G., Suppressed Jahn-Teller Distortion in MnCo(2) O(4) @Ni(2) P Heterostructures to Promote the Overall Water Splitting. *Small*, **2020,** *16*, 2001856.

14. Wei, X.; Zhang, Y.; He, H.; Peng, L.; Xiao, S.; Yao, S.; Xiao, P., Carbon-incorporated porous honeycomb NiCoFe phosphide nanospheres derived from a MOF precursor for overall water splitting. *Chem Commun (Camb)*, **2019,** *55*, 10896-10899.

15. Sivanantham, A.; Ganesan, P.; Shanmugam, S., Hierarchical NiCo2S4Nanowire Arrays Supported on Ni Foam: An Efficient and Durable Bifunctional Electrocatalyst for Oxygen and Hydrogen Evolution Reactions. *Advanced Functional Materials*, **2016,** *26*, 4661-4672.